AIAA Aviation
16-20 June 2014, Atlanta, GA
20th AIAA/CEAS Aeroacoustics Conference

Phased-array measurements of full-scale military jet noise

Blaine M. Harker[1], Kent L. Gee[2], Tracianne B. Neilsen[3]
Brigham Young University, Provo, UT, 84602

Alan T. Wall[4]
Air Force Research Laboratory, Wright-Patterson Air Force Base, OH, 45433

and

Michael M. James[5]
Blue Ridge Research and Consulting, LLC, Asheville, NC, 28801

Beamforming techniques for aeroacoustics applications have undergone significant advances over the past decade to account for difficulties that arise when traditional methods are applied to distributed sources such as those found in jet noise. Nevertheless, successful source reconstructions depend on array geometry and the assumed source model. The application of phased-array algorithms to ground array measurements of a full-scale tactical jet engine at military and afterburner engine conditions yield different source reconstructions. A deconvolution approach for the mapping of acoustic sources (DAMAS) is utilized to remove array effects seen in conventional beamforming and allows for improved interpretation of results. However, the distributed nature of the jet noise source, as well as large correlation lengths at low frequencies, can result in inaccurate source locations and/or amplitudes for both conventional beamforming and DAMAS. Results using DAMAS-C, an extension of DAMAS, indicate the degree of source correlation within the military aircraft noise. Source reconstructions on the jet centerline for different one-third octave band frequencies confirm the greater source correlation at low frequencies. These preliminary results represent the first implementation of DAMAS-C on full-scale jet noise data.

Nomenclature

$\mathbf{A}$	=	Point-spread functions matrix
$\mathbf{b}$	=	Total beamform response vector
B	=	Beamwidth of the array
CSM	=	Cross spectral matrix
c	=	Ambient sound speed
δ	=	Scaling factor to limit residual component variability
e_{mn}	=	Steering element
$\mathbf{e_n}$	=	Steering vector
f	=	Frequency
$G_{mm'}$	=	Cross spectral elements
H	=	Conjugate matrix transpose
k	=	Wavenumber
m	=	Measurement location index
M	=	Number of measurement locations
n	=	Scan point index
N	=	Number of scan points
$q_n^{(s)}$	=	Residual component at each iteration s

[1] Graduate Student, Dept. of Physics and Astronomy, N283 ESC, AIAA Student Member.
[2] Associate Professor, Dept. of Physics and Astronomy, N283 ESC, AIAA Senior Member.
[3] Part-Time Assistant Professor, Dept. of Physics and Astronomy, N283 ESC, AIAA Member.
[4] Postdoctoral Research Fellow, Battlespace Acoustics Branch, AFRL 711 HPW/RHCB, AIAA Member.
[5] Senior Principal Engineer, 29 N Market St, Suite 700, AIAA Member.

r_{mn} = Distance from measurement m to scan location n
s = Iteration number
T = Matrix transpose
$\mathbf{x}$ = Vector of monopole source strengths
Δx = Spacing between scan points
X_{nn_0} = Cross-source amplitude from n and n_0
$x_n^{(s)}$ = Source strength at scan point n and iteration s
Y_n = Beamformed response for scan point n

I. Introduction

Success in future jet noise reduction efforts require an improved understanding of the noise source characteristics. However, direct measurement of flow parameters are difficult for full-scale measurements due to the heated, turbulent nature of the flow field. Array-processing techniques, e.g., beamforming, are commonly used as a means of estimating the distributions of the jet noise sources from indirect measurements. Beamforming has been applied in multiple contexts to aeroacoustics problems[1-4] though care must be taken to address potential challenges and limitations that the signal processing can introduce. Array geometry and placement are key factors that influence resolution of the reconstruction, presence of grating lobes and other artifacts that create challenges and limitations. When array measurements are not optimized, array deconvolution methods have shown promise in improving beamforming results.[5] In addition to the array and processing considerations, choice of the assumed reconstruction model must be evaluated such that the model represents the physical properties of the source mechanisms. For example, the correlated, distributed source nature of jet noise violates the common beamforming assumption that the source consists of incoherent monopoles. This effect has been noted to result in inaccurate source levels and source locations in the reconstructions.[6-8]

Beamforming techniques for aeroacoustics applications have undergone significant advances over the past decade to account for difficulties that arise when beamforming techniques are applied to distributed sources as those found in jet noise. Venkatesh *et al.*[9] developed a phased-array method to calculate an average source strength over a distributed region. Brooks and Humphreys[5] produced the deconvolution approach for the mapping of acoustic sources (DAMAS), which allows for the removal of the array point-spread function, thus improving spatial resolution and providing accurate source level estimates. Further deconvolution methods introduced, including DAMAS2[10] and LORE,[11] have also been effective in this endeavor. Dougherty and Podboy[12] applied beamforming methods with a time-domain deconvolution algorithm (TIDY) to a laboratory-scale engine. While addressing the distributed nature of the source, these algorithms still assume that the source region consists of incoherent monopoles.

The implicit assumptions of the underlying source models influence jet noise source characterization efforts. Suzuki and Colonius[13] modeled instability waves of near-field jet measurements using an Eigen function approach. Kœnig *et al.*[14] used a wavepacket model to reconstruct far-field measurements of a subsonic cold laboratory jet. Du and Morris[15] used a wavepacket model to image source information from simulated jet noise data. Lee and Bridges[2] applied conventional beamforming techniques to jet noise using a far-field polar and linear array to reconstruct an equivalent line source at the nozzle and along the jet axis. Although some methods expand upon the incoherent monopole assumption, including the work by Suzuki[16] to beamform dipole sources, source correlation is particularly difficult to account for using conventional beamforming methods. Attempts to account for source correlation include Brooks and Humphreys extension of the DAMAS algorithm to allow for correlated and partially-correlated sources (DAMAS-C), although at a high computational cost.[7] This method differs from DAMAS in that no assumption of incoherent monopoles is made. CLEAN-SC has also been introduced with similar results.[17] These applications to simulations and laboratory-scale jets have helped develop the methods.

There have been relatively few application of phased-array analyses to full-scale jet noise. Schlinker *et al.*[18] measured noise from a supersonic tactical engine using a 30 microphone phased array located within the maximum radiation region and 16 nozzle diameters from the jet centerline. Source distributions as a function of engine condition were presented and comparisons were made to a laboratory-scale jet. Brusniak *et al.*[19] used a polar array, a linear array and a multi-arm spiral to measure jet noise sources at the nozzle exit and downstream of a full-scale commercial grade engine. Measurements from the arrays were compared for consistency and conventional beamforming applied to the jet centerline. However, neither of these analyses applied a deconvolution to the beamforming results for improved resolution. Dougherty and Mendoza[20] used a 100 foot radius polar arc array in measurements of a full-scale engine and applied DAMAS and CLEAN-SC to engine and jet noise beamforming results to show a higher resolution image using both methods and a reduction in sidelobes using CLEAN-SC. Padois *et al.*[21] tested a hybrid beamforming

method is introduced and briefly compared with DAMAS and CLEAN-SC on a full-scale aero-engine. While many of these methods have been proposed to improve computation time, the authors have not found application of the originally proposed method, DAMAS-C, in a full-scale jet noise analysis.

The focus of this paper is the preliminary implementation of DAMAS and DAMAS-C to the noise measured on a line array of ground-based microphones in the vicinity of an F-22A Raptor. In the present measurement, DAMAS is applied to remove array effects introduced from array geometry and provide a more accurate and higher resolution linear reconstruction estimate. Because of a high variability in the spectral content around the jet as a function of spatial position, the array length is investigated. While the assumption of incoherent monopoles is potentially reasonable for the modeling of sideline radiation, this is not true for the frequencies producing the dominant radiation. Wall *et al.*[22] showed that for full-scale tactical engines in the peak-frequency region, measured acoustic correlation lengths near the source span multiple wavelengths. Thus, source correlation must be taken into account to produce physically meaningful results. To more accurately reconstruct sources spanning large coherence lengths, DAMAS-C is applied to deconvolve correlated sources. A generalized model of arbitrarily correlated monopoles along the jet axis is assumed in DAMAS-C and applied to F-22 measurements. Preliminary results confirm that localization techniques need to include the partially correlated, extended nature of the jet noise sources to yield physically reasonable estimates of the source distribution.

II. Methods

Before applying phased-array methods to the noise measured near the F-22, a discussion of the methods is presented. A brief introduction to conventional beamforming is given, and the DAMAS algorithm summarized. The array effects, which convolute conventional beamforming results of the source region are mitigated by means of the DAMAS algorithm while still assuming incoherent monopoles. The application of both conventional beamforming and DAMAS to simulated fields illustrates the consequences of the assumption of uncorrelated sources that underlies many beamforming methods and provides perspective for evaluating the F-22 results.

Because turbulent mixing noise from the F-22 is a partially correlated source, we introduce cross-beamforming and apply the DAMAS-C algorithm to investigate source correlation features. These methods are also applied to simulated array measurements, calculated from both correlated and uncorrelated monopole source distributions, to evaluate the ties between source correlation and phased-array results. The numerical simulations show the efficacy and limitations of both DAMAS and DAMAS-C in the reconstruction of correlated and uncorrelated source distributions as well as the utility of these methods over conventional beamforming. From this investigation, implications regarding the application of these methods to jet noise are presented.

A. Conventional Beamforming

The deconvolution approach for the mapping of acoustic sources (DAMAS) was first proposed by Brooks and Humphreys.[5] An overview of the method is provided to facilitate the interpretation of the results. For a more detailed account, refer to Ref. [5] and Ref. [10]. Measurements of an acoustic field are taken using an array of M microphones (see Figure 1), which need not be uniformly spaced. The auto-spectra and cross-spectra of the measurements are used to create the cross-spectral matrix, given by

$$\mathrm{CSM} = \begin{pmatrix} G_{11} & \cdots & G_{1M} \\ \vdots & \ddots & \vdots \\ G_{M1} & \cdots & G_{MM} \end{pmatrix}, \tag{1}$$

where G_{ij} represents a cross-spectral element for a given frequency, f. A steering vector is used to adjust the phase and amplitude of each array element so that the beamformed result appropriately reconstructs amplitudes at a specific location. For a source distribution of uncorrelated monopoles, the desired scanning region of interest consists of a grid of N equispaced locations shown in Figure 1. The steering vector to a scanning location n is defined as

$$\mathbf{e}_n = [e_{1n}\, e_{2n} \ldots e_{Mn}]^T, \tag{2}$$

where T signifies transpose, and the steering elements from each array element m are given as

$$e_{mn} = r_{mn} \exp(jkr_{mn}). \tag{3}$$

Here, r_{mn} is the distance from measurement m to scan location n. This is similar to a free-field Green's function for a monopole source, with the amplitude-scaling factor inverted to represent reverse propagation. The resulting beamformed response for scan location n is given by

$$Y_n = \frac{\mathbf{e}_n^H \mathrm{CSM} \mathbf{e}_n}{M^2}, \tag{4}$$

where H signifies a Hermitian transpose. In many applications, such as those where there is significant self-noise (e.g. wind) in the array measurements, diagonal removal of the CSM is commonly employed to reduce the noise and improve beamformed results. This practice is omitted here due to the high signal-to-noise ratio measured at the array. Furthermore, it was found that in numerical simulations, diagonal removal tended to increase the overall sidelobe levels in the beamformed results, reducing the resolution of low-level features. The dispersion of energy is a common consequence in array processing methods, with the array point-spread function determining the array imaging quality. Poorly designed arrays suffer from a high degree of spreading from a point source while carefully designed arrays can reduce this effect.

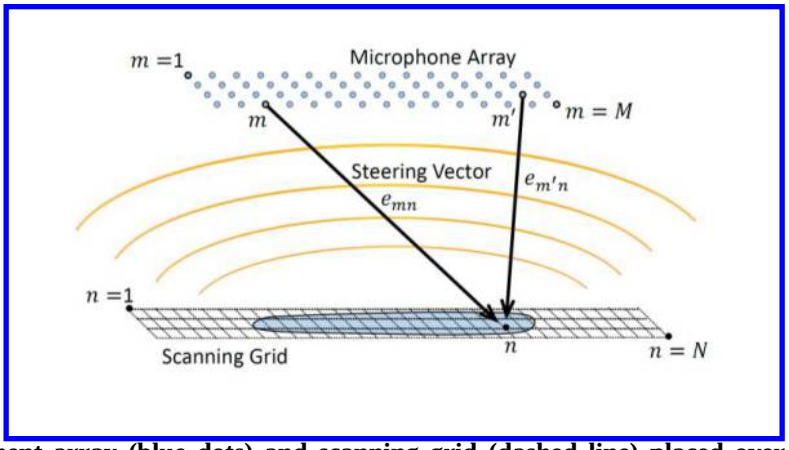

Figure 1. Measurement array (blue dots) and scanning grid (dashed line) placed over source distribution (illustrated in blue).

B. DAMAS Algorithm

DAMAS is employed to deconvolve the array effects in conventional beamforming from the original source properties. The problem is cast into a linear system of equations,

$$\mathbf{A}\,\mathbf{x} = \mathbf{b}, \tag{5}$$

where the DAMAS algorithm assumes that incoherent monopoles, each with a different complex amplitude, comprise the original source region. In Equation 5, $\mathbf{x}$ is a vector of monopole source strengths located at each scanning grid point n as $\mathbf{x} = [x_1\ x_2\ \ldots x_N]^T$. The vector $\mathbf{x}$, when convoluted by $\mathbf{A}$, produces the beamform response at each scanning grid location, grouped into a vector as $\mathbf{b} = [Y_1\ Y_2\ \ldots Y_N]^T$. The matrix $\mathbf{A}$ is formed by combining anticipated convolution data, with each matrix column representing the beamform output of a single monopole at position n, vectorized into a column format. It is calculated by

$$\mathbf{A}_{nn'} = \frac{\mathbf{e}_n^H\,[\cdot]_{n'}\,\mathbf{e}_n}{M^2} = \frac{\mathbf{e}_n^H\left[\mathbf{e}_{n'}^{-1}\left(\mathbf{e}_{n'}^{-1}\right)^H\right]\mathbf{e}_n}{M^2} = \frac{\left|\mathbf{e}_n^H\mathbf{e}_{n'}^{-1}\right|^2}{M^2}, \tag{6}$$

with $[\cdot]_{n'}$ representing the CSM of a single monopole located at n'. The inverse steering vector,

$$\mathbf{e}_n^{-1} = [e_{1n}^{-1}\ e_{2n}^{-1}\ \ldots e_{Nn}^{-1}]^T, \tag{7}$$

is formed by combining inverse steering elements

$$e_{mn}^{-1} = \frac{1}{r_{mn}} \exp(jkr_{mn}). \tag{8}$$

The linear system in Eq. (5) is solved iteratively using a Gauss-Seidel type relaxation method with a non-negativity constraint. At each iteration step, s, a residual component $q_n^{(s)}$ is calculated for each location n. It is defined as

$$q_n^{(s)} = \sum_{j=1}^{n-1} A_{nj}\, x_j^{(s+1)} + \sum_{j=n}^{N} A_{nj} x_j^{(s)} - Y_n, \tag{9}$$

where A_{nj} are elements of $\boldsymbol{A}$, x_j are elements of $\boldsymbol{x}$, and Y_n are components of $\boldsymbol{b}$. The source strength vector is initialized as $x_n^{(s)} = 0$, although it has been shown that beginning with a more likely estimate of the initial source distribution reduces the necessary number of iterations to converge on a solution.[23] As each residual term is updated, the solution for the source strength, $x_n^{(s+1)}$, is also updated as

$$x_n^{(s+1)} = \max\left(x_n^{(s)} - \frac{\delta\, q_n^{(s)}}{A_{nn}}, 0 \right), \tag{10}$$

where a non-negativity constraint is enforced to ensure all source strengths are physically significant. The equation can be further simplified since $A_{nn} = 1$. To reduce the variability from iteration to iteration and smooth the convergence of **x**, a scale factor δ is utilized such that $\delta \leq 1$, and it is set to 0.01 for the cases shown in this paper. Iterations are repeated until the residual converges to a minimum value. In this paper, the number of iterations is typically set to 1000. The rate of convergence is typically frequency dependent, with higher frequencies converging more quickly. DAMAS results also depend on the ratio of the spacing between scanning points, Δx, to the beamwidth of the array, B, measured as the diameter of the 3 dB down region of a point source reconstruction. For example, depending on the choice of $\Delta x/B$, a simple source may be distributed across multiple scanning points resulting in a distribution of the original source strength over the multiple points. Brooks and Humphreys in Ref. [5] give a suitable range as $0.05 \leq \Delta x/B \leq 0.20$. In the following results, $\Delta x/B = 0.20$ is used, unless otherwise noted.

To illustrate the advantages of DAMAS, an application of both conventional beamforming and DAMAS to the numerical case of a single point source are provided. The source is centered to a fifty-element receiver array in a free space, shown in Figure 2(a). The array is designed similar to the array used in the full-scale measurements. A one-dimensional scanning grid region spanning 5.0 m to 20.0 m and spaced such that $\Delta x/B = 0.20$ is also displayed in Figure 2(a). The results at 300 Hz are given in Figure 2(b), with the location and amplitude of the point source indicated by the red circle. The conventional beamforming algorithm (black) represents the array point-spread function and yields a relatively wide central lobe, whose amplitude at the peak output matches the original source level, and grating lobes. When DAMAS (blue) is applied, the sidelobe levels are significantly reduced and a narrow point source is reconstructed. The level of the DAMAS reconstruction is lower than the point source because of the fine resolution of the scanning grid; the reconstruction of the source is distributed across at least three scanning points. The combined amplitude across these points is 94.2 dB re 20 μPa: only a 0.2 dB error from 94.0 dB re 20 μPa assigned as the point source amplitude at this single frequency.

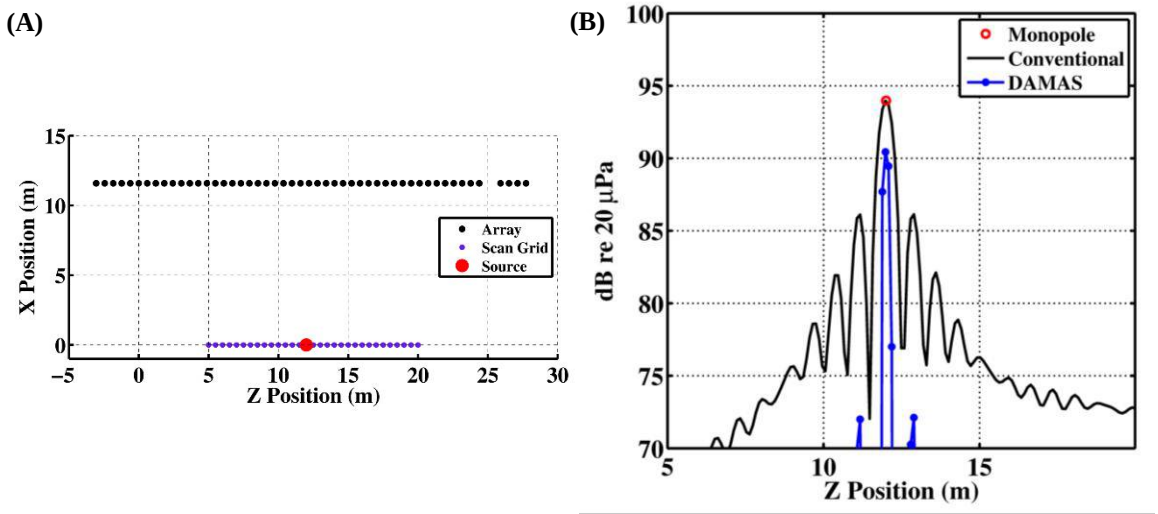

Figure 2. (A) Geometric configuration of receiving array and source reconstruction grid for the numerical example of a single monopole. (B) Conventional beamforming (black) and DAMAS results (blue) for one frequency of the single monopole.

For more complicated sources, especially those whose regions span multiple wavelengths and exhibit some degree of correlation, the application of conventional beamforming and DAMAS is not straightforward. To provide a benchmark for these sources, we construct line arrays of monopoles, where the monopole strength is normally distributed along the array and the sources are either correlated or uncorrelated. The same receiving array shown in Figure 2(a) is used and in each case the line array is located at X = 0 and Z = 0 - 10 m. The conventional beamforming and DAMAS results at 300 Hz are shown in Figure 3. The spacing of line array elements is set equal to the spacing of scanning grid elements to more easily compare the source and reconstruction levels. For the uncorrelated collection of monopoles, individual sources do not constructively add in the field and consequently, the beamforming output is successfully able to reconstruct general locations and relative distributions of the source, although significant array effects increase the resultant amplitude and spread of the source. DAMAS on the other hand, more accurately matches both the location and the amplitudes. Because the source distribution is not centered on the array, there is a slight skew in the DAMAS results in the $-Z$ direction and residual DAMAS components at $Z < 0$ m. However, the results illustrate the ability of DAMAS to improve conventional beamforming results after array effects are considered. The result for the correlated line array is different, as shown in Figure 3(b). Here, the line source is steered to 125° relative to the –Z axis such that the peak levels across the receiving array are at its center. The correlated line array elements add constructively to produce a field that is difficult for conventional beamforming algorithms to reconstruct, since they rely on the assumption of uncorrelated monopoles. Consequently, the conventional beamforming results in Figure 3(b) are higher in amplitude and more steeply varying compared with the original source distribution. In the DAMAS results, the reconstructed source distribution levels are closer to the original source levels, although the distribution is compressed and levels are much higher in amplitude. Although not shown here, it was found that a similar correlated distribution with a source directivity of 90° from the –Z axis produced a less accurate reconstruction because the peak levels across the microphone array are off-center, providing less overall measurement coverage to the entire array.

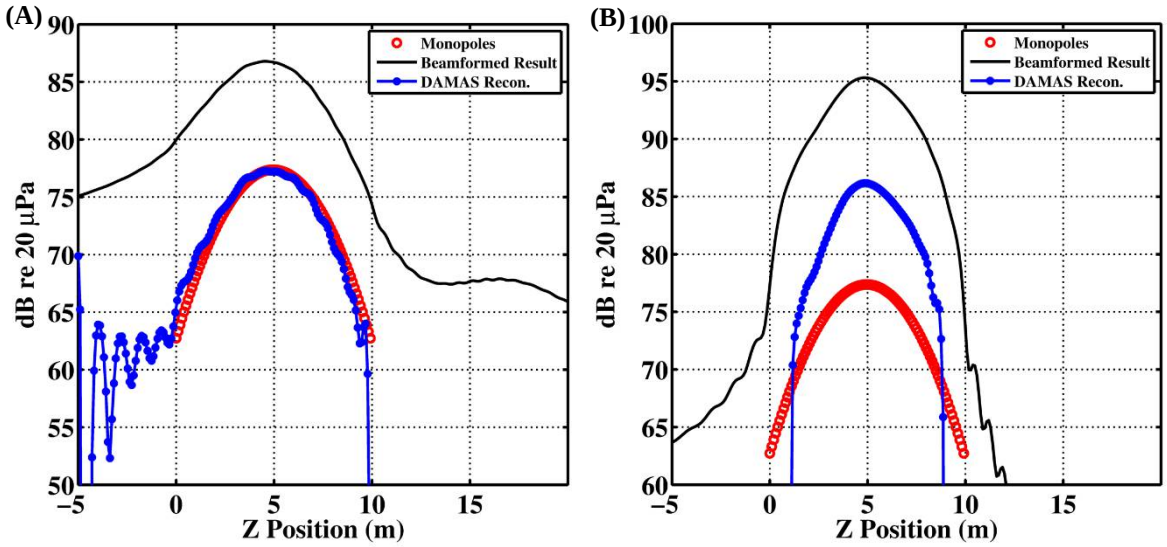

Figure 3. (A) Normal distribution of uncorrelated monopoles and (B) correlated monopoles (shown in red) with beamforming results (black) and the DAMAS reconstructions (blue).

C. Cross-Beamforming

While DAMAS is successful at significantly improving reconstruction resolution for uncorrelated sources, its application to source correlation produces inaccurate results in amplitude and source distributions. DAMAS-C is an extension of DAMAS, which provides information on the source correlation characteristics. However, this method has been seldom used in the literature due to its high computational costs. Hence, this preliminary study focuses on one-dimensional source reconstructions, which typically have much lower computational costs by requiring fewer scanning grid elements. The following mathematical development is summarized from Ref. [7], although it has been recast in a manner similar to Ref. [10] to incorporate a residual component.

A cross-beamform technique is an extension to conventional beamforming because it does not assume a specific type of correlated source model *a priori*. In a manner similar to DAMAS, a scanning grid is created and cross-beamform output, a measure of the cross-response between scanning elements n and n_0 is

$$Y_{nn_0} = \frac{\mathbf{e}_n^H \,\mathrm{CSM}\, \mathbf{e}_{n_0}}{M^2}. \tag{11}$$

A significant response is produced when correlation between presumed sources at scanning points n and n_0 exists and a low response when little correlation exists. For computational efficiency, it is convenient to note that $Y_{n_0 n} = Y^*_{nn_0}$, where * signifies complex conjugate. The cross-beamform algorithm provides a suitable means whereby correlation between adjacent and nonadjacent source distributions are found. Just as in the case of conventional beamforming, these results are convoluted by array effects, which limit the successful interpretation of results.

D. DAMAS-C Algorithm

DAMAS-C is an extension of DAMAS, which deconvolves the cross-beamform output to remove array effects and provide a more accurate reconstruction of source properties. In a similar manner as DAMAS, the problem is cast as a linear system of equations:

$$\sum_{n_0', n'} A_{n_0 n, n_0' n'} X_{n_0' n'} = Y_{n_0 n,} \tag{12}$$

where $X_{n_0' n'}$ represents the cross-source amplitudes each point n_0' and n' in the field, and $Y_{n_0 n}$ represents the cross-beamform output at points n and n_0. It should be noted that $X_{n_0 n} = X^*_{nn_0}$. The 4-dimensional matrix $A_{n_0 n, n_0' n'}$

encapsulates all possible contributions due to possible source correlation between sources n_0' and n' when measured jointly at points n and n_0, respectively. It is given by

$$A_{n_0 n, n_0' n'} = \frac{\mathbf{e}_{n_0}^H [\cdot]_{n_0' n'} \mathbf{e}_n}{M^2}, \tag{13}$$

where the equivalent cross-spectral matrix attributed to source contributions from n_0' and n' is given as

$$[\cdot]_{n_0' n'} = \begin{bmatrix} \left(e_{1n_0'}^{-1}\right)^* e_{1n'}^{-1} & \cdots & \left(e_{1n_0'}^{-1}\right)^* e_{Mn'}^{-1} \\ \vdots & \ddots & \vdots \\ \left(e_{Mn_0'}^{-1}\right)^* e_{1n'}^{-1} & \cdots & \left(e_{Mn_0'}^{-1}\right)^* e_{Mn'}^{-1} \end{bmatrix} = \left(\mathbf{e}_{n_0'}^{-1}\right)^* \left(\mathbf{e}_{n'}^{-1}\right)^T. \tag{14}$$

The cross-response of n and n_0 resulting from presumed sources at n_0' and n' will result be significant if source correlation exists between both scanning element pairs. It should be noted that

$$A_{n_0 n, n_0' n'} = A_{n n_0, n' n_0'}^* \ , \tag{15}$$

which greatly reduces the time necessary to calculate this matrix. Typically, **A** requires the highest computational costs and a significant amount of computer memory, typically on the order of $16 \cdot N^4$ bytes for double-precision complex elements of **A**. For example, a scanning grid with 150 elements requires the matrix **A** to require about 8.1 GB of computer memory.

The source strength matrix is initialized in a manner similar to DAMAS, with $X_{nn_0}^{(0)} = 0$. With each iteration, the residual is calculated as

$$q_{nn_0}^{(s)} = \sum_{k=1}^{n} \sum_{l=1}^{n_0 - 1} A_{nn_0, kl} X_{kl}^{(s+1)} + \sum_{k=n}^{N} \sum_{l=n_0}^{N} A_{nn_0, kl} X_{kl}^{(s)} - Y_{nn_0}, \tag{16}$$

with the first term in each residual given as

$$q_{11}^{(s)} = \sum_{k=1}^{N} \sum_{l=1}^{N} A_{11, kl} X_{kl}^{(s)} - Y_{11}. \tag{17}$$

For each iteration, the source matrix is updated for diagonal matrix terms by,

$$X_{nn}^{(s+1)} = \max\left(X_{nn}^{(s)} - \delta \cdot \mathrm{Re}\left(q_{nn}^{(s)}\right), 0\right), \tag{18}$$

and for off-diagonal terms by

$$X_{nn_0}^{(s+1)} = \max\left(X_{nn_0}^{(s)} - \frac{\delta \, q_{nn_0}^{(s)}}{\left|A_{nn_0, nn_0}\right|}, 0\right), \tag{19}$$

with the constraint

$$\left|X_{nn_0}^{(s+1)}\right| \leq \sqrt{X_{nn}^{(s)} X_{n_0 n_0}^{(s)}}. \tag{20}$$

The non-negativity constraint on the diagonal terms is similar to the DAMAS algorithm and provides physically meaningful source amplitudes. The constraint on off-diagonal terms follows from the argument in Ref. [7] that source

correlation between points n and n_0 will be related by $X_{nn_0} = \gamma_{n_0 n}\sqrt{X_{nn}}\sqrt{X_{n_0 n_0}}$, where $\gamma_{n_0 n}$ is the complex coherence between regions n and n_0. Thus, it is expected that $|X_{n_0 n}| \leq \sqrt{X_{n_0 n_0} X_{nn}}$. The scaling factor δ is again used as in the DAMAS algorithm to provide smoother convergence. Typically DAMAS-C requires much more computational cost than DAMAS, and therefore few applications are found in the literature. However, the algorithm is robust and does not assume *a priori* a source and, thus, provides more accurate results in the case of correlated source distributions.

Little has been published in regards to methods of iterating across elements n and n_0 over each iteration step. Iteration generally proceeds across the scanning grid so that residual energy is transferred evenly to adjacent scanning grid elements. For a one-dimensional DAMAS problem, iterations are carried out by Ref. [10] in a left to right, then right to left iteration scheme. This is similarly conducted for the one-dimensional iterations in the current DAMAS applications. In this paper, iteration for a DAMAS-C algorithm, which incorporates an additional dimension to the reconstruction region, proceed via the scheme illustrated in Figure 4. This attempts to distribute residual energy equally without creating regions in the scanning grid where leftover residual is unnecessarily gathered.

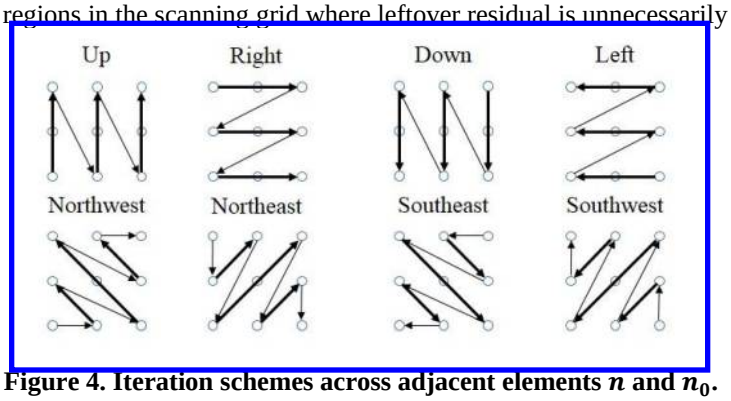

Figure 4. Iteration schemes across adjacent elements n and n_0.

Because jet noise is generated by extended, partially correlated sources, DAMAS-C is more applicable than DAMAS because it does not assume the reconstruction of incoherent monopoles. To illustrate how DAMAS-C treats uncorrelated and correlated sources, we return to the test cases described in Sec. IIB. Specifically, cross-beamforming and DAMAS-C are applied to the uncorrelated and correlated source distributions to understand the abilities and remaining limitations of DAMAS-C. The results are shown in Figure 5. In Figure 5(a), the cross-beamform results of the uncorrelated source distribution are presented. The diagonal elements represent $Y_{nn} = Y_n$ and are similar to the beamformed results in Figure 3(a). The off-diagonal elements, $Y_{n_0 n}$, show the relationship between source reconstructions at n_0 and n. Although the source distributions are uncorrelated, the self-correlation the distribution is not completely negligible. The cross-beamform results show a small degree of correlation between sources, marked by the lower amplitude levels adjoining the off-diagonal terms of each distribution. This was also seen by Brooks and Humphreys in the cross-beamform results for a monopole.[7] DAMAS-C results in Figure 5(b) reveal significantly less off-diagonal results due to the uncorrelated nature of the sources. The correlated source distribution results are given in Figure 5(c-d). The cross-beamform results show significant levels of self-correlation across the source distribution. The DAMAS-C results refine the features shown in the cross-beamform results and emphasize the amount of correlation present due to all source contributions. The differences in the off-diagonal elements in the DAMAS-C results for the correlated source distribution as compared to the uncorrelated case indicate significantly more correlation between the sources and provide confidence that DAMAS-C delivers information regarding not only source location but also source correlation. Due to the existence of off-diagonal elements and the chosen method to iterate through the DAMAS-C algorithm, the diagonal elements may differ slightly from the DAMAS results given in Figure 3.

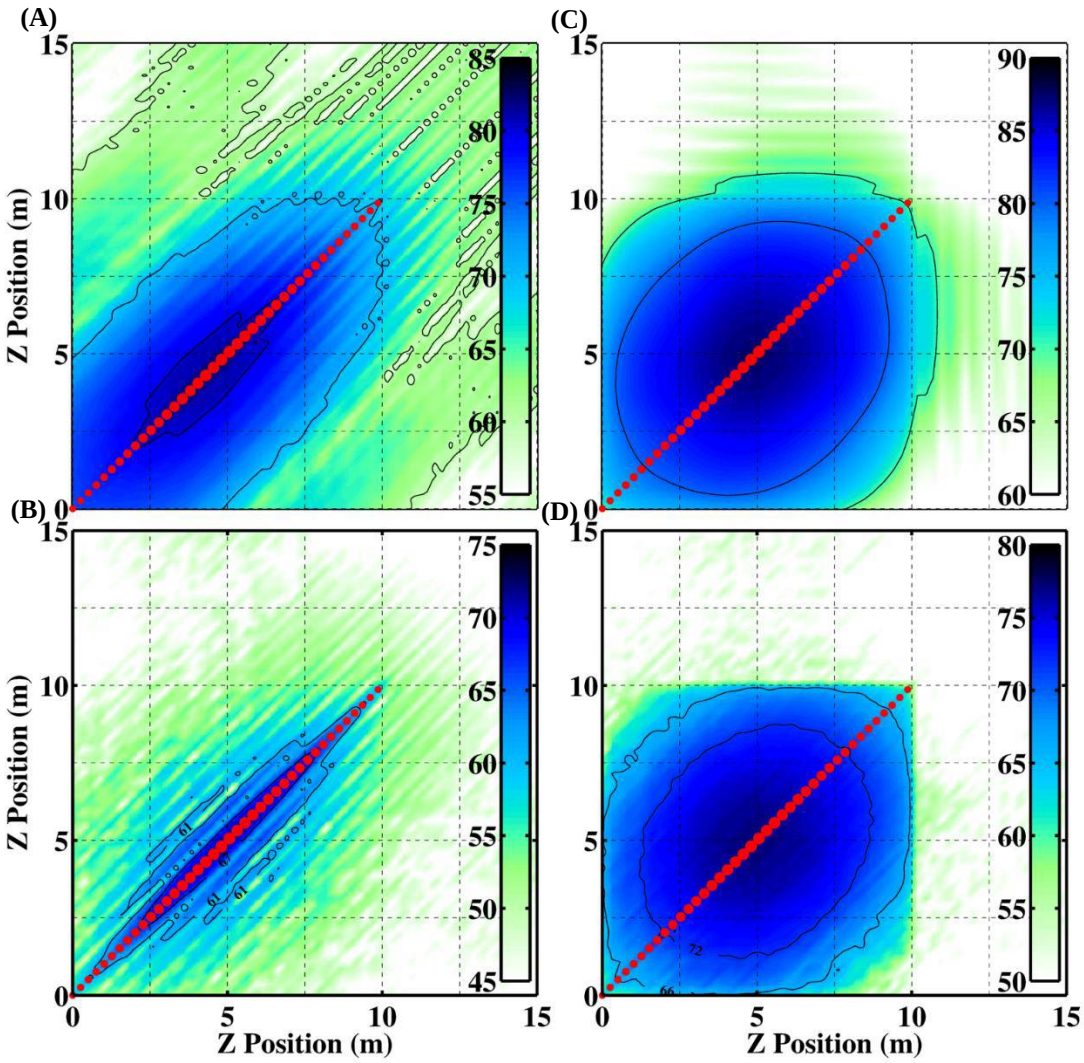

Figure 5. A) Cross-beamform results and B) DAMAS-C results of an uncorrelated normal distribution C) Cross-beamform results and D) DAMAS-C results of a correlated normal distribution. Scales are in dB re 20 μPa.

III. Results

Measurements were made of a Pratt and Whitney model F119-PW-100 turbofan engine installed on the Lockheed-Martin/Boeing F-22A Raptor, conducted July 2009 at Holloman Air Force base [see Figure 6(a)]. The measurements were made jointly by the Air Force Research Laboratory, Blue Ridge Research and Consulting, LLC, and Brigham Young University. One of the engines on the tied-down aircraft was operated at four engine conditions while the other was held at idle. An array of 50 GRAS 6.35-mm and 3.18-mm microphones was placed on the ground 11.6 m from the centerline of the jet axis. A detailed description of the experiment is explained Ref. [24], and the spectral variation of the measured sound as a function of angle is shown in Ref. [25].

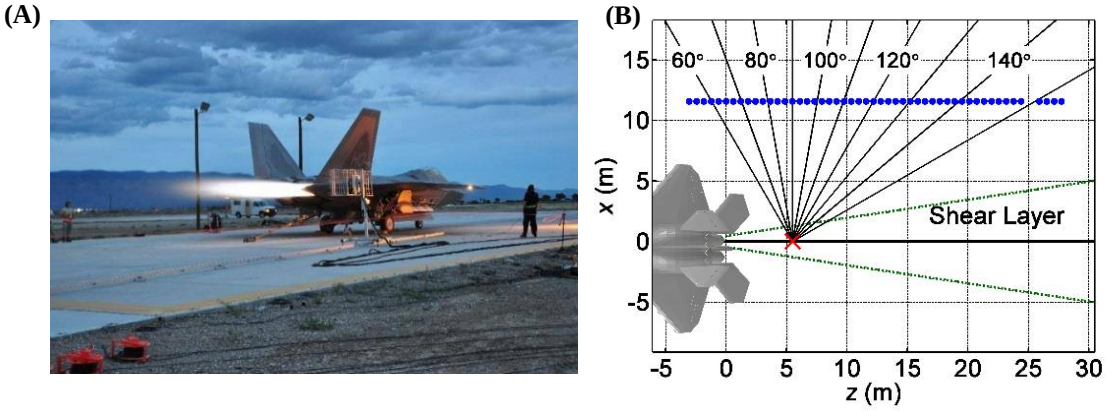

Figure 6. A) Photograph of the F-22 measurements taken July 2009. B) Schematic of the measurements. The ground array (blue dots) was located at the edge of the concrete in the photograph.

The ground array element spacing is 0.61 m, and the array spans 30 m. Array measurements are beamformed to the axis of the jet centerline, shown in Figure 6(b), with the scanning grid density held constant such that $\Delta x/B = 0.2$ across all frequencies. The beamforming results for a case when the engine was operated at military power (100% ETR) are shown in Figure 7(a) for one-third octave bands, and the corresponding DAMAS results are given in Figure 7(b). The one-third octave band source reconstructions are computed by averaging over multiple narrow-band frequencies in the one-third octave. For this experiment, the auto-spectral values of the cross-spectral matrix were included when the beamform output was calculated, as it was found to improve low-level resolution. The beamform output shows the large distributed jet source region, which has a peak source region that shifts as a function of frequency. This source shift is markedly pronounced between 100 Hz and 200 Hz as it varies both in peak source location and source width. As frequency increases, the peak source region shifts upstream until it reaches a limiting value centered at about 2.0 m from the jet nozzle. The source size also compresses as a function of frequency with the largest source distribution occurring at or below 100 Hz. At low frequencies, the array geometry is such that there is a large distribution spread in the beamform output that is unreasonable for physically meaningful results. These array effects typically results when there is insufficient variation in point-spread function at these frequencies to properly render accurate results. As frequency increases, the equivalent source region is compressed to a location smaller and closer to the jet nozzle. The overall results are consistent with those taken by Schlinker *et al.*[18] of a comparable full-scale military engine, who showed a maximum source location centered approximately 4-6 nozzle diameters downstream for frequencies between 250 Hz and 400 Hz. The results are also comparable to the location found by Brusniak *et al.*,[19] who localized jet noise sources centered about 3-4 nozzle diameters downstream for a full-scale commercial grade engine.

As seen in the numerical examples described in Sec. II, the DAMAS technique provides a clearer source reconstruction than traditional beamforming (See Figure 7). Even though at high frequencies, grating lobes are introduced, as evidenced in the DAMAS reconstruction beginning around 400 Hz, the main source region is well separated from these grating lobes. The strongest source reconstruction region from DAMAS occurs at 100 Hz and peaks at approximately 130 dB re 20 μPa. The DAMAS equivalent source distribution at 100 Hz is centered approximately 5.9 m downstream of the jet nozzle and the 3dB down region is 6.3 m wide from 2.7 m to 9.0 m downstream the nozzle exit. At 315 Hz, the peak is farther upstream at about 3.3 m with a 3 dB region spanning 3.1 m from 1.9 m to 5.0 m. At low frequencies, the DAMAS results remove much of this large source distribution region, but not all the energy correctly converges to the main source region, as evidenced by the residual energy located at the edge of the scanning grid below about 90 Hz. However, the peak locations across the valid frequency range of this array, correspond fairly well with those estimated by other methods, including the laser probe spatial distributions published by Tam *et al.*[26]

However, the variation in the extent of the source region with frequency obtained by DAMAS is not as significant as expected from other analyses.[27] As shown in the preceding numerical examples, this contracted apparent source region likely occurs because correlated sources are not accurately represented when reconstructed and deconvolved using DAMAS. DAMAS compresses the extent of correlated sources while conserving the overall distributed source energy. For frequencies where source coherence across the measurement plane is high, it is expected that the DAMAS results are likely compressed, while sources with lower coherence are more likely well represented by DAMAS. Previous studies have shown coherence lengths across the microphone array range from 3-10 m at 100 Hz and from

1-3 m at 315 Hz.[22] Hence, the equivalent source region estimates obtained when DAMAS is applied to the F-22 noise are likely compressed at frequencies below 300 Hz due to the underlying assumption of uncorrelated sources.

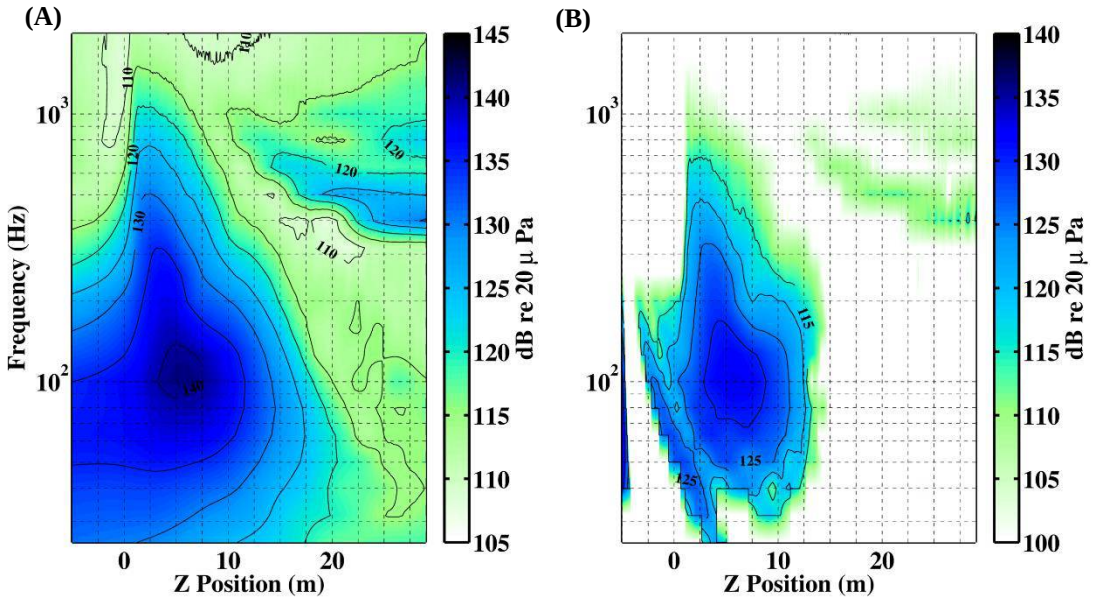

Figure 7. A) Beamforming results and B) DAMAS results of F-22 measurements at military power, measured from ground array and steered to jet center axis.

Similar results are seen when the F-22 was operated at afterburner (>100% ETR), with a few differences likely due to the increased temperature and thrust. As shown in Figure 8, a downstream shift in the peak of approximately 1-2 m occurs at most frequencies. For example, the DAMAS source distribution at 100 Hz peaks around 7.3 m downstream and the 3 dB down region spans 6.3 m and extends from 4.2 m to 10.5 m downstream, while at 315 Hz the peak is centered at 4.5 m with a 3 dB down region spanning 5.4 m from 2.3 m to 7.7 m. The strong shift in source width and location seen at the military case is not so pronounced here, with only a more gradual shift occurring at about 20 Hz. DAMAS yielded consistent source regions at 100 Hz of 6.3 m for both conditions, and an expansion of the source region at 315 Hz from 3.1 m in the military case to 5.4 m at afterburner. As with the military case, the equivalent source regions obtained by DAMAS are likely contracted at lower frequencies due to the partially correlated nature of jet noise. For frequencies above 400 Hz, the center of the equivalent source region converges to between 2-5 m downstream.

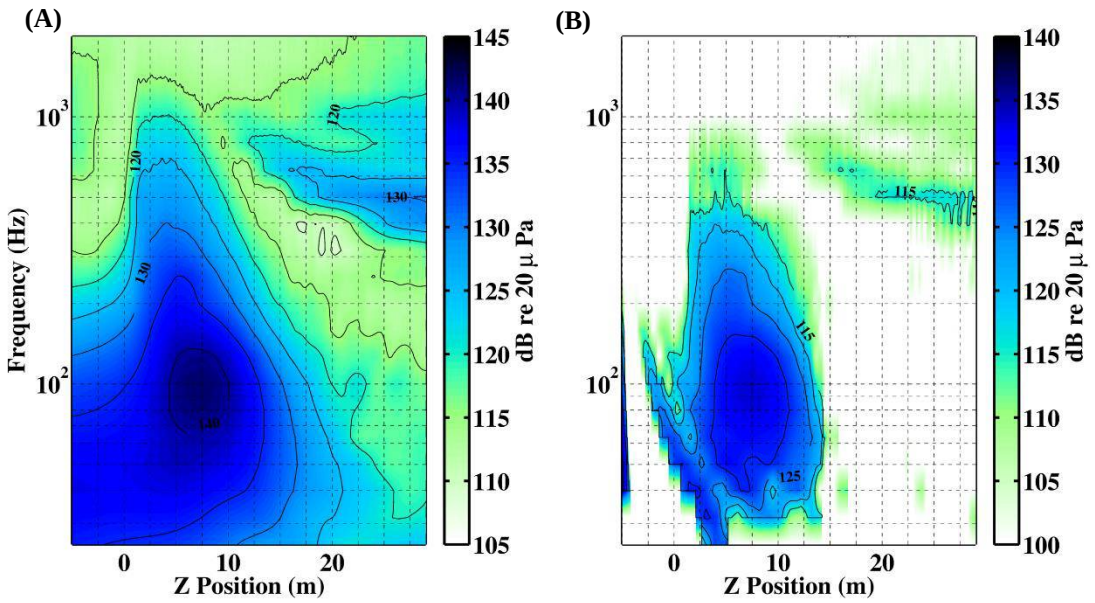

Figure 8. A) Beamforming results and B) DAMAS results of F-22 measurements at afterburner power, measured from ground array and steered to jet center axis.

Neilsen *et al.*[25] showed a large variation in spectral content as a function of look direction along the ground array. In particular, low frequency noise dominates farther downstream, but higher frequencies are more prominent to the sideline of the nozzle. Because the measurement array spans a large aperture parallel to the jet axis, the features from sideline and downstream regions are combined into one beamform output when using all 50 microphones. To illustrate the effects of using this large aperture on beamforming results and to examine the ability of DAMAS to identify different source regions, the algorithms were applied to data from two halves of the ground-based array while the F-22 was operated at military power. The resulting beamformed output and DAMAS reconstructions across one-third-octave bands are shown in Figure 9. The top/bottom two plots are produced when the upstream/downstream half of the array are used (i.e., the first/last twenty-five elements of the ground array).

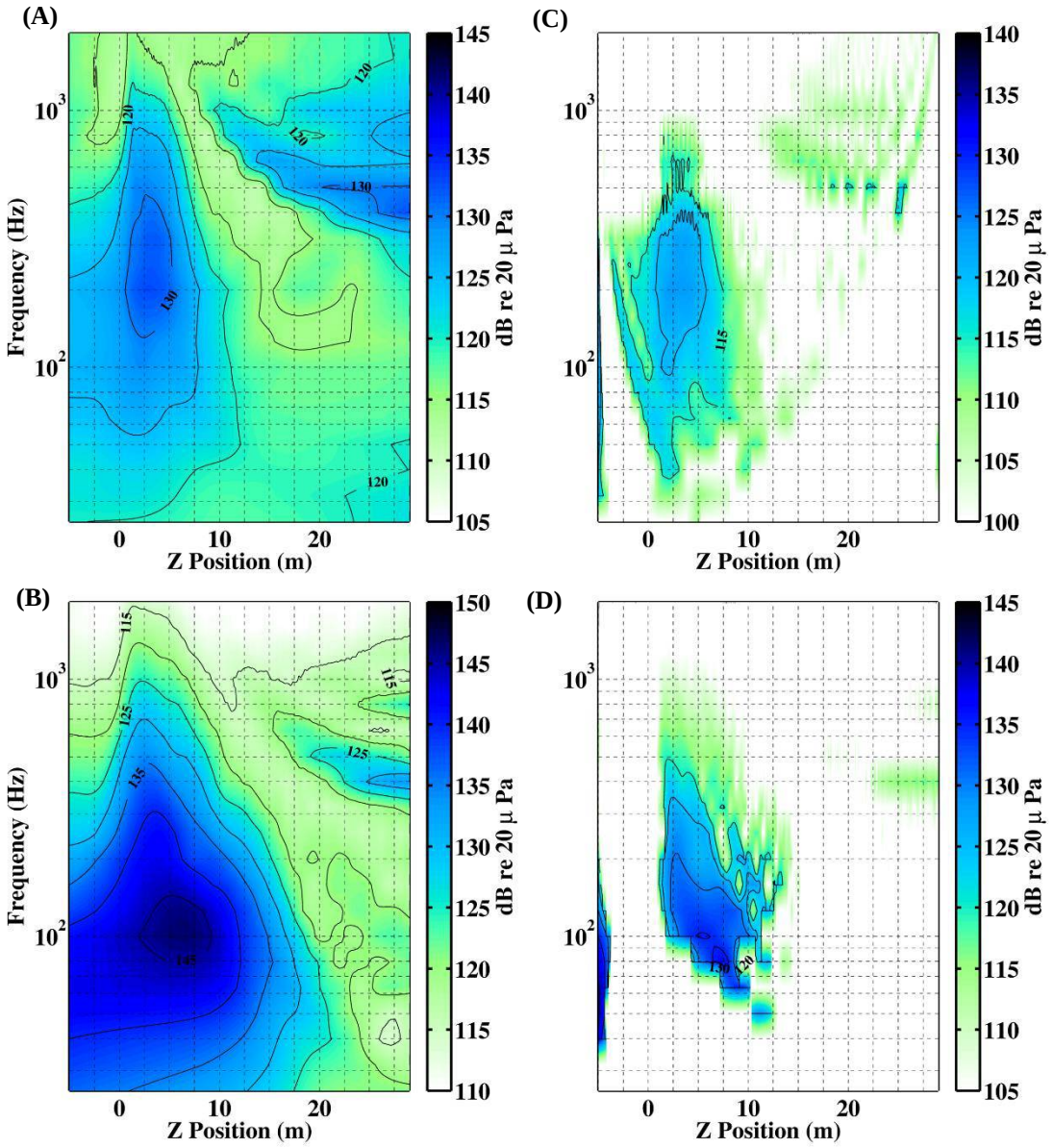

Figure 9. A) Beamforming results of F-22 measurements at military power, measured from the upstream half of ground array and steered to jet center axis as well as B) its DAMAS reconstruction. C) Beamforming results at military power using downstream half of ground array and D) its DAMAS reconstruction.

The difference in beamform output for the upstream and downstream subarrays shows significant distinction between the radiation measured at each respective region. Because the upstream subarray detects less overall energy than the downstream subarray, the corresponding results are markedly lower. The upstream array localized the equivalent source region close to the nozzle exit across all frequencies, with a wider extent at low frequencies than high. This is particularly evident in the DAMAS results, which remove some of the side features resulting from array effects. The main source distribution exhibits more symmetry compared with the results from the full array. The secondary lobe seen in the DAMAS results which is more upstream and which is also visible in Figure 7(b) and Figure 8(b) seems to be related to the upstream array measurement or array geometry, hence, it likely that this feature is not physically meaningful. The results for the downstream array show greater variation across frequencies in both peak location and extent. The locations of the peak beamform output are, in most cases, slightly downstream from what was found when the entire 50-microphone array and have greater variation at the low frequencies. In addition, at the lowest frequencies the spatial extent of the equivalent source region is substantially contracted. This contraction and

the larger variation in peak region could be due to the isolation of the more strongly correlated portions of the waveform that are prominent in the main radiation lobe that crosses the downstream location of the subarray. Artifacts such as the strong secondary source located outside the main source region and about 2 m farther downstream, beginning at about 125 Hz, are likely related to the limited aperture of the subarray.

As shown above, the correlated nature of the source region may contribute to inaccurate results using conventional beamforming methods and DAMAS. Thus, DAMAS-C is implemented to provide information as to the relative correlation of the source region. The DAMAS-C results are shown below for one-third octave band frequencies of 125 Hz, 315 Hz, and 800 Hz at military engine condition in Figure 10. To reduce computation time, the scanning grid region and/or the scanning grid spacing were altered so as to allow for reasonable computation times, using Intel Xeon CPU's at 2.4GHz (2 Processors, each with 8 threads) and 50GB of available RAM. DAMAS-C results were computed in MATLAB using parallel methods and typical times were on the order of 24 hours for a one-third octave band measurement comprised of multiple narrow-band computations. Contour lines are spaced at 6 dB increments from the maximum plotted value. While the cross-beamform results, also shown in Figure 10, are computed using $\Delta x/B = 0.20$, the scanning grid spacing for DAMAS-C was altered for the 315 Hz and 800 Hz cases to 0.6 at 315 Hz (0.3 m spacing) and 1.5 at 800 Hz (0.3 m spacing). This allows for practical computation times for calculating the matrix **A**, which quickly become unreasonable at higher frequencies.

At 125 Hz, the cross-beamform results show a large correlation source region centered at about 6 m downstream and extending about 20 m, over a 12 dB down width measured from the peak. This region over which the source is correlated is reduced considerably when deconvolved via DAMAS-C. The DAMAS-C estimated source size spans a large extent from approximately from 2.5 m to 10 m with a 6 dB drop from the maximum result, and spans from approximately 1 m to 14 m across a 12 dB drop from the maximum. At 315 Hz, the cross-beamform results show a much narrower source region than at 100 Hz with more variation in the off-diagonal terms. DAMAS-C, however, reduces the 315 Hz cross-beamform results to a small region spanning from approximately 1 m to 8 m downstream. The maximum source region, centered at about 4 m downstream, shows a 6 dB drop in amplitude for the off-diagonal elements spanning at about 3 m, measured from the maximum source region. Residual components are also present in terms off-diagonal from the main source region. In general, the source correlation is much lower than that found at 125 Hz. At 800 Hz, the maximum source region is moved farther upstream, and the DAMAS-C results looked markedly similar to those from the uncorrelated normal distribution shown in Figure 5. Source regions located at 12 m and 27 m are due to grating lobes, thus, correlation between these source regions is expected.

Although source correlation is accounted for using DAMAS-C, the possibility of distortion due to the correlated nature of the radiation may still be of concern when interpreting the accuracy of the results. While the integrated source energy should be correct and relative source location accurate, the source region found by DAMAS-C may be slightly contracted due to the correlated nature of the source.

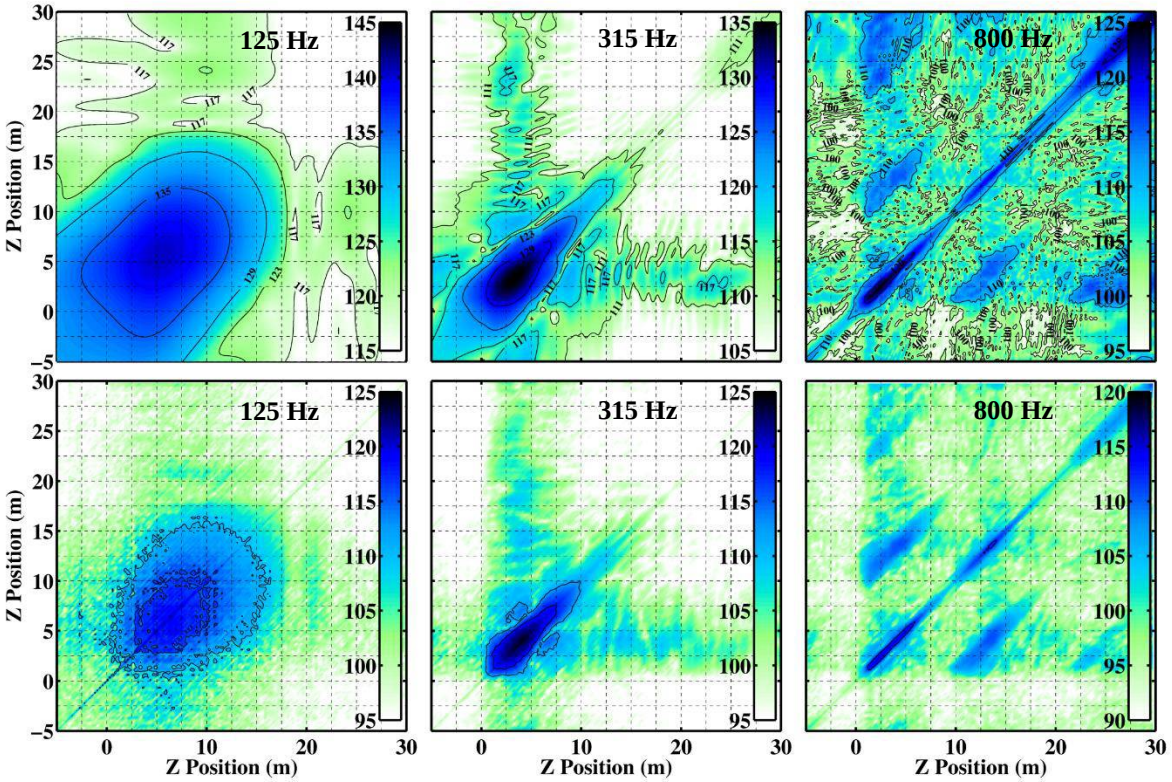

Figure 10. (Top) Cross-beamform results and (Bottom) DAMAS-C results for 125 Hz, 315 Hz, and 800 Hz military condition at one-third octave band frequencies. Contour lines are spaced at 6 dB increments. Scales are in dB re 20 μPa.

IV. Conclusions

The application of phased-array techniques and deconvolution techniques to acoustic measurements in the vicinity of an F-22 represent the first such investigation on a full-scale high performance military aircraft noise. Beamforming results, from a ground-based, 50 microphone sideline array, as well as deconvolution results using DAMAS and DAMAS-C, have been presented for the F-22 when one engine was operated at military and afterburner engine conditions. Compared to traditional beamforming, DAMAS removes the array artifacts and provides for better interpretation of the equivalent source reconstruction. When the entire array, spanning 30 m, is used in the algorithms, a distributed frequency-dependent source region is identified. The source region moves downstream 1-2 m for afterburner as compared to the military engine condition. The use of subarrays in DAMAS allows for the separation of source features that potentially originate from the sideline and/or downstream region. When the upstream region is used as input, the peak frequency is higher and closer to the engine nozzle than when the entire array in used.

DAMAS-C is an extension of DAMAS that not only yields an equivalent source region but also indicates source correlation. Numerical studies have shown that beamforming reconstructions based on signals from correlated source are compressed in comparison with those from uncorrelated source distributions. Thus, when phased-array techniques, which are based upon the assumption of uncorrelated monopoles, are applied to partially correlated sources, such as jet noise, the calculated source distributions may be inaccurate without proper methods to account for source correlation. DAMAS-C is one way to evaluate the degree of correlation in acoustic sources. Additional work is necessary to relate DAMAS-C results to source characteristics, such as coherence lengths. Nevertheless, the preliminary application of DAMAS-C to the F-22 data indicates that there is significant correlation across the extended source region at lower frequencies and less correlation at higher frequencies. These results agree with prevailing theories of jet noise and shed light on the intricacies of applying phased-array methods to jet noise sources.[25, 26]

Acknowledgments

The authors would like to thank Chris Bahr, Thomas Brooks and Charlotte Whitfield of NASA Langley as well as Karl Weidermann for initial resources and direction in the implementation of DAMAS and DAMAS-C. The authors gratefully acknowledge funding for this analysis from the Office of Naval Research. The measurements were funded by the Air Force Research Laboratory through the SBIR program and supported through a Cooperative Research and Development Agreement (CRDA) between Blue Ridge Research and Consulting, Brigham Young University, and the Air Force. Distribution A: Approved for public release; distribution unlimited. Cleared 05/14/2014; 88ABW-2014-2306.

References

[1]W. M. Humphreys, W. W. Hunter, K. R. Meadows, and T. F. Brooks, "Design and use of microphone directional arrays for aeroacoustic measurements," AIAA Paper 98-0471, 1998.

[2]S. S. Lee and J. Bridges, "Phased-Array Study of Dual-Flow Jet Noise: Effect of Nozzles and Mixers," AIAA Paper 2006-2647, 2006.

[3]D. Papamoschou, P. J. Morris, and D. K. McLaughlin, "Beamformed flow-acoustic correlations in high-speed jets," AIAA Paper 2009-3212, 2009.

[4]J. Panda and R. Mosher, "Use of a Microphone Phased Array to Determine Noise Sources in a Rocket Plume," AIAA Paper 2011-974, 2011.

[5]T. F. Brooks and W. M. Humphreys, "A deconvolution approach for the mapping of acoustic sources (DAMAS) determined from phased microphone arrays," *Journal of Sound and Vibration* **294**, 856-879 (2006).

[6]W. C. Horne, J. A. Hayes, S. M. Jaeger, and S. Jovic, "Effects of distributed source coherence on the response of phased arrays," AIAA Paper 2000-1935, 2000.

[7]T. F. Brooks and W. M. Humphreys Jr, "Extension of DAMAS phased array processing for spatial coherence determination (DAMAS-C)," AIAA Paper 2006-2654, 2006.

[8]R. P. Dougherty, "Improved generalized inverse beamforming for jet noise," *International Journal of Aeroacoustics* **11**, 259-290 (2012).

[9]S. R. Venkatesh, D. R. Polak, and S. Narayanan, "Beamforming algorithm for distributed source localization and its application to jet noise," *Aiaa Journal* **41**, 1238-1246 (2003).

[10]K. Ehrenfried and L. Koop, "Comparison of iterative deconvolution algorithms for the mapping of acoustic sources," *Aiaa Journal* **45**, 1584-1595 (2007).

[11]P. A. Ravetta, R. A. Burdisso, and W. F. Ng, "Noise Source Localization and Optimization of Phased Array Results (LORE)," (2006).

[12]R. P. Dougherty and G. G. Podboy, "Improved phased array imaging of a model jet," AIAA Paper 2009-3186, 2009.

[13]T. Suzuki and T. Colonius, "Instability waves in a subsonic round jet detected using a near-field phased microphone array," *Journal of Fluid Mechanics* **565**, 197-226 (2006).

[14]M. Kœnig, A. V. Cavalieri, P. Jordan, J. Delville, Y. Gervais, and D. Papamoschou, "Farfield filtering and source imaging of subsonic jet noise," *Journal of Sound and Vibration* **332**, 4067-4088 (2013).

[15]Y. Du and J. M. Philip, "Numerical simulation of the effect of a low bypass cooling stream on supersonic jet noise," AIAA Paper 2014-1402, 2014.

[16]T. Suzuki, "L1 generalized inverse beam-forming algorithm resolving coherent/incoherent, distributed and multipole sources," *Journal of Sound and Vibration* **330**, 5835-5851 (2011).

[17]P. Sijtsma, "CLEAN based on spatial source coherence," *International Journal of Aeroacoustics* **6**, 357-374 (2007).

[18]R. Schlinker, S. Liljenberg, D. Polak, K. Post, C. Chipman, and A. Stern, "Supersonic Jet Noise Characteristics & Propagation: Engine and Model Scale," AIAA Paper 2007-3623, 2007.

[19]L. Brusniak, J. Underbrink, E. Nesbitt, D. Lynch, and M. Martinez, "Phased array measurements of full-scale engine exhaust noise," AIAA Paper 2007-3612, 2007.

[20]R. Dougherty and J. Mendoza, "Phased Array Beamforming with 100-Foot Polar Arc Microphones in a Static Engine Noise Test," AIAA Paper 2008-51, 2008.

[21]T. Padois, A. Berry, P.-A. Gauthier, and N. Joshi, "Beamforming matrix regularization and inverse problem for sound source localization : application to aero-engine noise," AIAA Paper 2013.

[22]A. T. Wall, K. L. Gee, T. B. Neilsen, and M. M. James, "On near-field acoustical inverse measurements of partially coherent sources," *Proceedings of Meetings on Acoustics* **11**, 040007 (2012).

[23]P. D. Robert, R. Rakesh Chandran, and R. Ganesh, "Deconvolution of Sources in Aeroacoustic Images from Phased Microphone Arrays Using Linear Programming," AIAA Paper 2013.

[24]A. T. Wall, K. L. Gee, M. M. James, K. A. Bradley, S. A. McInerny, and T. B. Neilsen, "Near-field noise measurements of a high-performance military jet aircraft," *Noise Control Engineering Journal* **60**, 421-434 (2012).

[25]T. B. Neilsen, K. L. Gee, A. T. Wall, and M. M. James, "Similarity spectra analysis of high-performance jet aircraft noise," *Journal of the Acoustical Society of America* **133**, 2116-2125 (2013).

[26]C. K. W. Tam, K. Viswanathan, K. K. Ahuja, and J. Panda, "The sources of jet noise: Experimental evidence," *Journal of Fluid Mechanics* **615**, 253-292 (2008).

[27]T. A. Stout, K. L. Gee, T. B. Neilsen, A. T. Wall, and M. M. James, "Intensity analysis of peak-frequency region in noise produced by a military jet aircraft," *Proceedings of Meetings on Acoustics* (Submitted 2014).